Development of a Lightweight LTO/Cu Electrode as a Flexible Anode *via* Etching Process for Lithium-Ion Batteries

Chih-Hung Chen,[⊥] Jian-Ming Chiu,[⊥] Indrajit Shown, and Chen-Hao Wang*

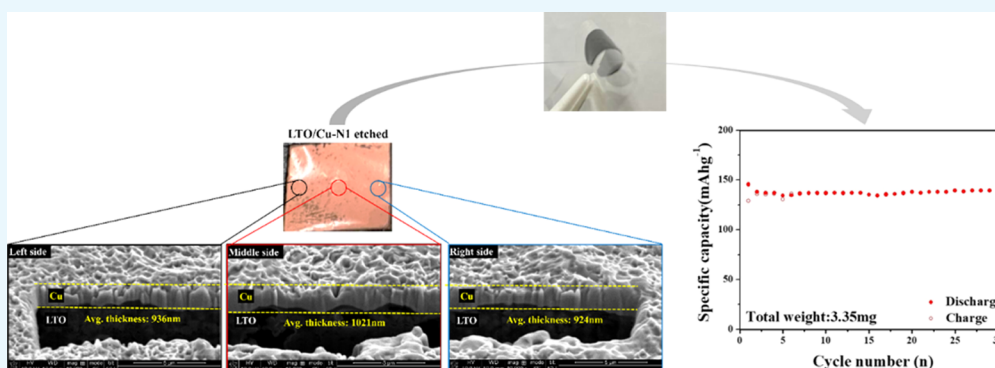Cite This: *ACS Omega* 2022, 7, 10205−10211

Read Online

ACCESS | Metrics & More | Article Recommendations | Supporting Information

ABSTRACT: In recent years, flexible energy storage devices have attracted the growing demand for flexible electronic systems. Therefore, research on reliable electrodes with high mechanical flexibility and good electronic and lithium-ion conductivity has become critical. Carbon-coated $Li_4Ti_5O_{12}$ (LTO) nanostructures find essential applications in high-performance lithium-ion batteries (LiBs). Nevertheless, the conventional copper current collector with a thickness of several micrometers accounts for a large proportion of the LiB, making the low-energy density LiB with much less flexibility. Here, hundred nm-thick (LTO/Cu) copper foil−LTO nanostructures are fabricated using a scalable and straightforward process which can be assembled into a film into a flexible, lightweight electrode by etching a conventional copper foil to form an ultra-thin copper layer for LIBs (<1 μm). This process provides essential flexibility to the as-prepared electrode and provides template support for simple fabrication. The LiB cell using the novel LTO/Cu as the anode exhibits an energy capacity of 123 mA h/g during 40 charge−discharge cycles at a 0.1C rate. Besides, the coulombic efficiency of the LiB using LTO/Cu remains over 99% after 40 cycles. These results show the uses of this novel anode and its potential in high-density and flexible commercial lithium-ion batteries.

1. INTRODUCTION

Interestingly, the actual energy capacity improvement of today's commercial lithium-ion batteries (LiBs) results from a reduced amount of inert materials (*e.g.*, binders and conductive particles) together with optimized cell design used by industries to provide the energy capacity.[1−3] In a commercial lithium-ion battery cell, the copper foil current collector coated with active anode materials has been used as a thin sheet anode with 12 μm thickness and 8.93 mg/cm^3 areal density. Moreover, a copper sheet/foil is a comparatively weighty component in a LiB and equivalent to the active material weight of the anode and contributes nearly 10% total weight of the battery.[4,5]

Although the current collector has the substantial weight of the battery cell, less effort has been attributed to the development of a lightweight current collector compared to other non-working components due to the high electrical conductivity of the copper foil. Various studies have shown that low-density conductive materials for the fabrication of a flexible current collector could provide significant lightweight and flexibility. As a result, carbon or conducting polymer electrodes

(paper or free-standing films) have been demonstrated as potential materials for flexible LiB applications.[6,7] Cui *et al.* have developed a lightweight current collector with a surface resistance around 5 Ω/sq based on a stainless-mesh-supported carbon nanotube (CNT)−silicon or a free-standing carbon nanotube−silicon composite. Although in Si nanowires, they reported that electron conductivity limits the lithiation process as compared with the lithium diffusion step, their flexible current collector showed noticeably higher surface resistance as compared to that of the metallic copper foil (1.4 m Ω/sq calculated using the resistivity of pure copper with 12 μm thickness).[8] Similarly, Li *et al.* have fabricated flexible electrodes
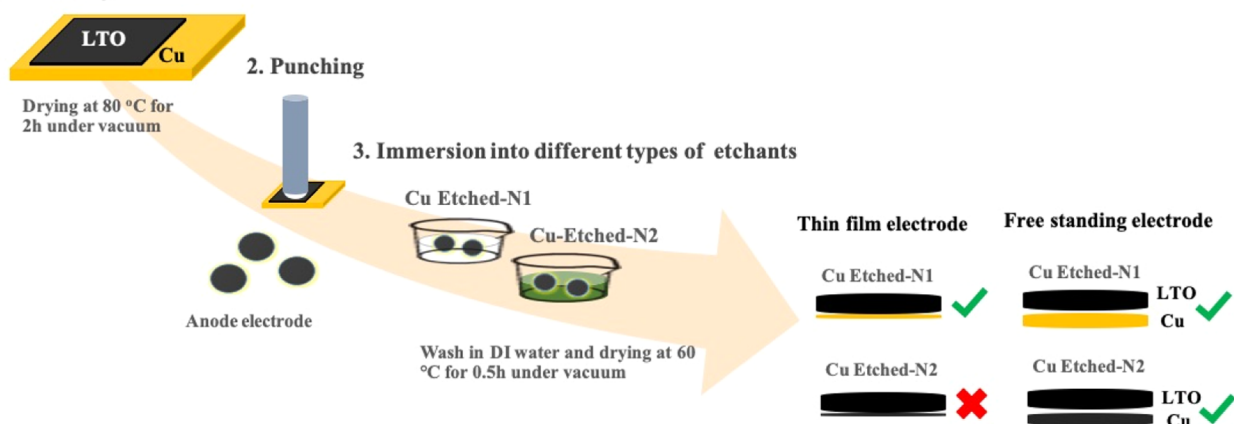
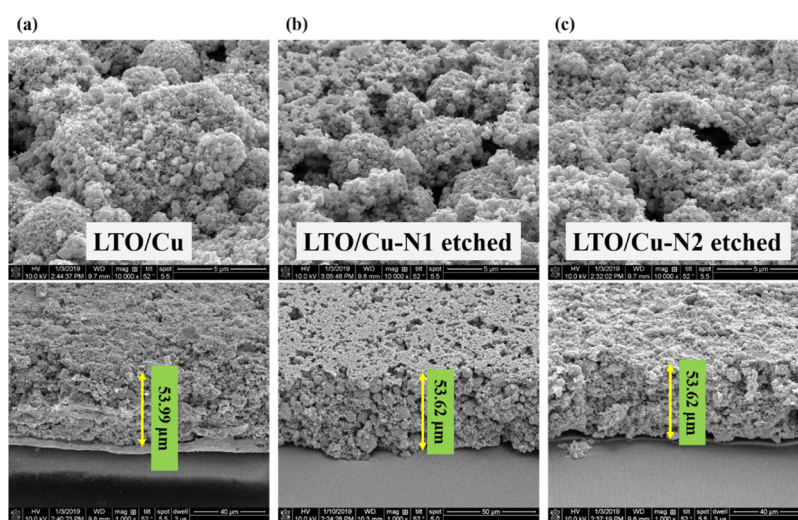**Figure 1.** Free-standing LTO/Cu electrode fabrication procedure.

Figure 2. SEM images of all the samples' top view (upper images) and cross-section view (lower images). (a) LTO/Cu, (b) LTO/Cu−N1 etched, and (c) LTO/Cu−N2 etched.
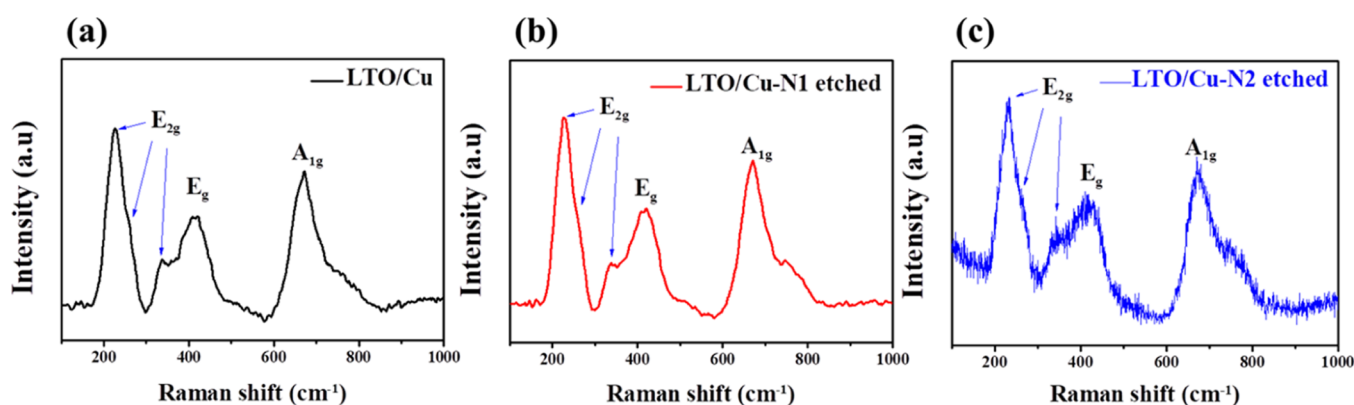

Figure 3. Raman spectra of (a) LTO/Cu, (b) LTO/Cu−N1 etched, and (c) LTO/Cu−N2 etched.

using $Li_4Ti_5O_{12}$ and graphene foam and showed a stable capacity with 55% retention of capacity at a 1 C-rate toward increasing current density up to a 20 C-rate.[9] Moreover, the reported electrode had high electronic conductivity, a large surface area, and high porosity, mainly due to the graphene foam. Koo *et al.* introduced PDMS and LiPON to fabricate a flexible all-solid-state system where the PDMS substrate provides significant flexibility and protects the cell from applied compressive force during the bending.[10] However, various factors like low robustness, mechanical strength, the high electrical resistance of electrodes, and lower loading of the active materials compared with conventional electrodes restrict the reported approaches for further implementation for LiB applications. Therefore, these methods need a complex prototype procedure and inclusive reliability analysis before use.[11−14]

To make the reliable and flexible LiB, the free-standing and flexible electrode for the LiB was employed by the $Li_4Ti_5O_{12}$ (LTO) deposited on an ultra-thin copper foil (≤ 1 μm thickness). First, LTO was cast on the conventional copper foil (LTO/Cu). Then, the sample was immersed into the specific etching solution to remove a large proportion of the copper foil, as shown in Figure 1. The thickness of the copper foil was less than or equal to 1 μm, but the etching solution had no bad influence on the performance of the LTO (LTO/Cu-etched). Thus, the energy density of the novel LTO/Cu-etched electrode is two times higher than that of the LTO/Cu electrode.

2. RESULTS AND DISCUSSION

2.1. Characterization of LTO/Cu and Etched LTO/Cu.
To exhibit the achievability of FS-LTO films as thin active anode material, the SEM images of pristine LTO/Cu, LTO/Cu−N1 etched, and LTO/Cu−N2 etched were executed to study the effects of the etchant variety and insertion of LTO on the microstructures of the free-standing electrodes, as shown in Figure 2. From the top view of all samples, they offer similar structures. From the cross-sectional view of all samples, they show almost the same thicknesses after the etching process. Therefore, those etchants will not destroy electrodes.

Also, we investigate the structural transformation of LTO during the etching process *via* Raman spectroscopy and XRD measurement. Figure 3a is the Raman spectrum of LTO/Cu. After being treated with different etchants, Figure 3b,c shows the Raman spectra of LTO/Cu−N1 etched and LTO/Cu−N2 etched, respectively. The peaks from LTO/Cu−N1 etched and LTO/Cu−N2 etched are consistent with those of LTO/Cu. However, the LTO/Cu−N2 etched part shows a weaker absolute intensity and a high noise ratio, which may be attributed to slight damage to the structure of some features. Figure S1 shows the results of XRD measurements, which provide insights into the crystal structure of LTO before and after etching with two different etching etchants. The results show that two different etchants do not destroy the crystal structure of LTO. To confirm if the titanium (Ti) element of LTO is dissolved by the etchant into the etch process, inductively coupled plasma optical emission spectrometry (ICP-OES) analyzes two etching solutions to qualify the amount of titanium. Table 1 shows that significantly lower

Table 1. Ti^{4+} in the Etching Solutions Using Different Etchants

| etchant	Ti^{4+} concentration (ppb)
Cu Etch-N1	166
Cu Etch-N2	14 810

concentrations of Ti^{4+} are obtained in the residual solution from the etchant of Cu Etch-N1 compared to that from the etchant of Cu Etch-N2. Table 1 shows the etchant of Cu Etch-N1, indicating that $FeCl_3$ in the etchant of Cu Etch-N2 is not suitable for the lightweight free-standing LTO electrode preparation procedure.

2.2. Battery Performance of LTO/Cu and Etched LTO/Cu.
We investigated the electrochemical behavior of pristine and different etchant-transferred LTO electrodes using 1 M $LiPF_6$ (in EC/DEC) as an electrolyte. The electrochemical potential profiles of LTO electrodes were cycled measured at the current density of the 0.1 C rate in the potential range of 1.3−2.5 V, as

shown in Figure 4. Figure 4a,c,e shows the capacities of the samples divided by LTO weight only. Figure 4b,d shows the capacities of LTO/Cu and LTO/Cu−N1 etched divided by the total weight of the electrode, but the capacity of LTO/Cu−N2 etched is too tiny to show herein. To clearly understand the capacities varied by the etchants, Table 2 shows the capacity changes of every sample at different cycles. LTO/Cu−N2 etched shows less capacity than LTO/Cu and LTO/Cu−N1 etched by approximately 150 mA h/g. The pristine LTO/Cu and LTO/Cu−N1 etched show good specific capacities in the range of around 150−160 mA h/g. These values are usually reached with commercial $Li_4Ti_5O_{12}$. In addition, the LTO/Cu−N1 etched effectively preserves the electrode impregnation sites with the etchant. As a result, the preliminary discharge capacity of the LTO/Cu−N1 etched was greater than that of pristine LTO/Cu by approximately 5 mA h/g.

To develop Li-ion battery devices with improved energy density, reducing the weight associated with the Cu foil is essential. The Cu foil with inherent high conductance, that is, 1.4 m Ω/sq, could effectively decrease the mass of the current collector to achieve a lightweight LiB. Figure 4d demonstrates that the capacity without etching the LTO electrode is stabilized around 70 mA h/g with a current rate of 0.1C after 40 cycles. Confirmation of the stability of the LTO electrode for 40 cycles was measured by XRD and SEM. The XRD patterns of pristine LTO exhibit three characteristic peaks at around 18, 35, and 43°, corresponding to (111), (311), and (400) diffraction planes of LTO, respectively. These three peaks are noticed at 2.5 V after 40 charge−discharge cycles, demonstrating that the LTO structure is sustained after 40 cycles. We also observed the SEM images of LTO electrodes before and after 40 charge−discharge cycles. However, their structures remain, resulting in stable capacitance (Figure S2). Figure 4e shows the cycling performance of an approximately 1 μm-thick LTO/Cu-etched film (Figure S3) at a rate of 0.1C. At the beginning of the charge−discharge cycle, the LTO electrode shows a discharge capacity of 129 mA h/g and remains at 123 mA h/g (or 95%) after 40 cycles. Followed by the charge−discharge cycle, it possesses a Coulombic efficiency of around 98% for the first cycle and greater than 99% throughout the rest cycles (based on the total weight of electrodes). The decrease in capacity is likely due to the contribution of the Cu foil, indicating that the suitable etchant reduces the Cu foil but does not destroy the electrode material and the current collector. Remarkably, the lightweight LTO/Cu−N1 etched film (total weight is 10.4 mg), related to the LTO anode on the Cu foil current collector (total weight is 20.2 mg), could considerably reduce around 50% weight of the positive side electrode (anode) in Li-ion batteries. Therefore, the lightweight electrode successfully improves the specific capacity nearly twice on the positive side electrode (anode).

After 40 cycles, CV curves were performed at a 0.1 mV s^{-1} scan rate to understand the electrochemical reaction during charge/discharge, as shown in Figure 5a. LTO/Cu and LTO/Cu−N1 etched show reversible redox peaks (reduction at about 1.50 V *vs* Li$^+$/Li) (oxidation peaks at about 1.75 V *vs* Li$^+$/Li), representing the lithiation and delithation process, respectively. The reversible redox peaks are the typical two-phase reaction of the redox couple of Ti^{3+}/Ti^{4+} during Li$^+$ insertion/extraction processes, as shown in the following reaction.[15]

$$Li_4Ti_5O_{12} + 3Li^+ + 3e^- \rightarrow Li_7Ti_5O_{12} \quad E^0 = 1.55 \text{ V}$$

(1)
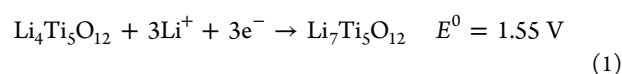
Figure 4. (a) LTO/Cu (LTO weight only), (b) LTO/Cu (total weight of the electrode), (c) LTO/Cu−N1 etched (LTO weight only), (d) LTO/Cu−N1 (total weight of the electrode), and (e) LTO/Cu−N2 etched (LTO weight only).

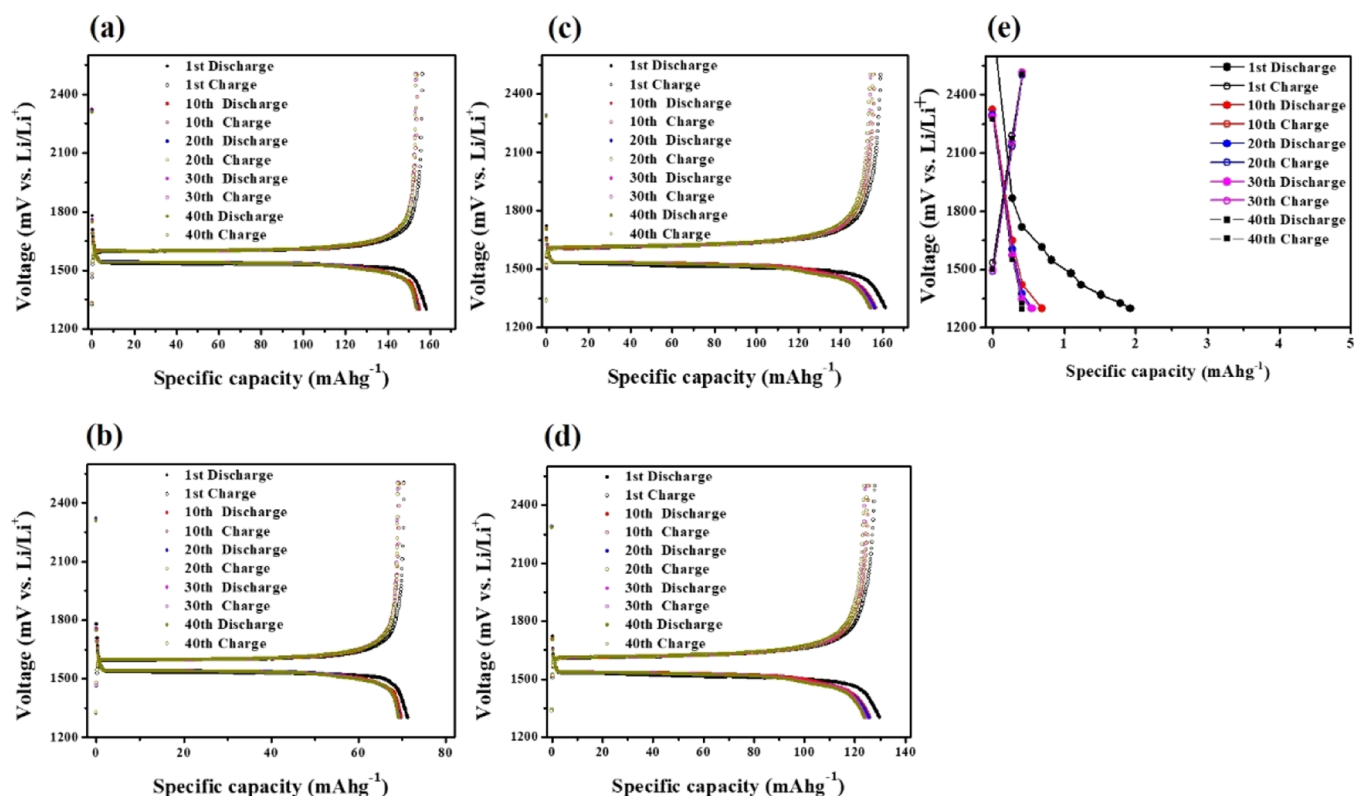**Table 2. Different Cycle Capacities with (a) LTO/Cu (LTO Weight Only), (b) LTO/Cu (Total Weight of Electrode), (c) LTO/Cu−N1 Etched (LTO Weight Only), (d) LTO/Cu−N1 (Total Weight of Electrode), and (e) LTO/Cu−N2 Etched (LTO Weight Only)**

| electrode	1st cycle capacity (mA h/g)		10th cycle capacity (mA h/g)		20th cycle capacity (mA h/g)		40th cycle capacity (mA h/g)	
	discharge	charge	discharge	charge	discharge	charge	discharge	charge
(a)	158.2	156.3	154.9	153.9	154.0	153.6	153.7	153.2
(b)	71.3	70.4	69.8	69.4	69.4	69.2	69.3	69.0
(c)	161.3	159.1	156.6	156.1	156.1	155.4	154.1	153.9
(d)	129.7	127.9	125.9	125.5	125.5	124.9	123.9	123.7
(e)	1.93	0.41	0.68	0.41	0.55	0.41	0.41	0.41
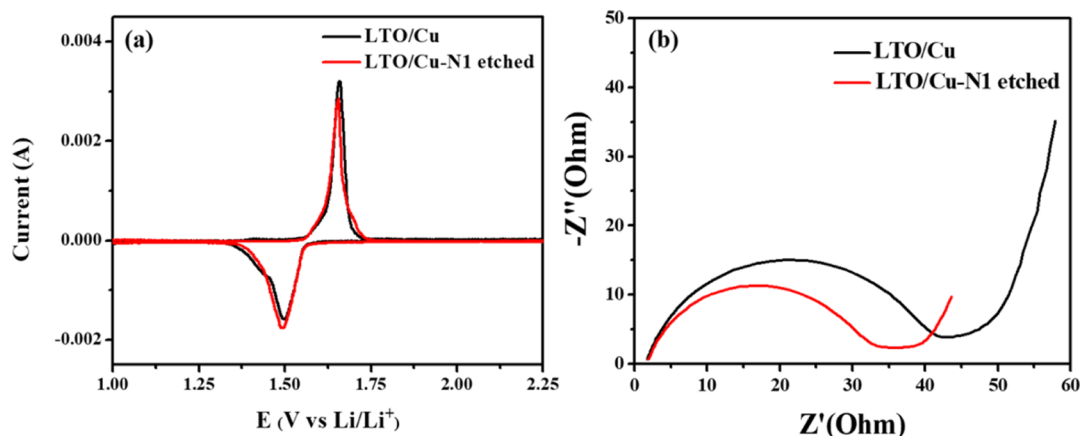
Figure 5. (a) Cyclic voltammograms of LTO/Cu and LTO/Cu_N1 etched from 1.0 to 2.25 V at a scan rate of 0.1 mV s^{-1}. (b) Impedance spectra of LTO/Cu and LTO/Cu−N1 etched measured after 40 cycles.

Figure 5b shows EIS analysis of LTO/Cu and LTO/Cu−N1 etched, which these two EIS curves show the semicircle shape of

the charge-transfer part and the straight line of the mass-transfer part at the high and medium frequency, respectively. As a
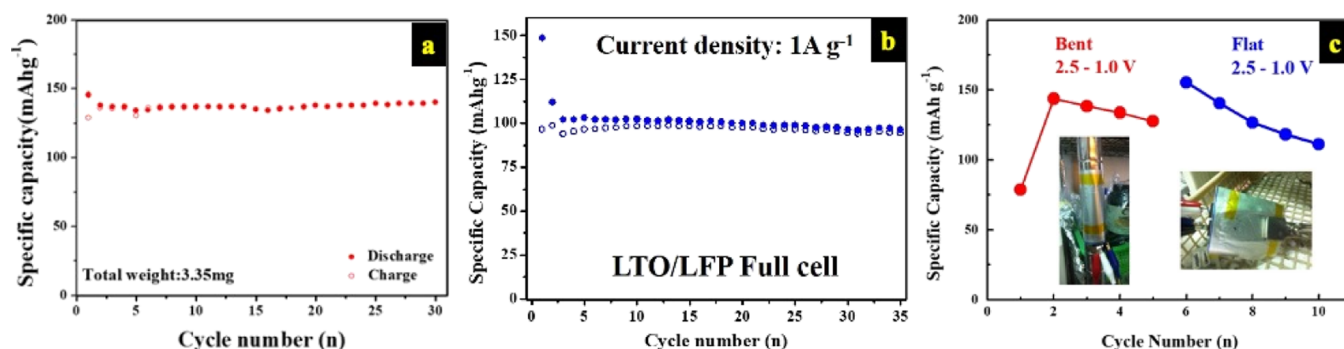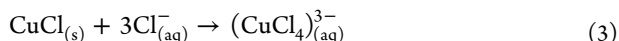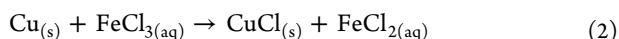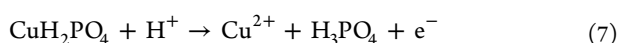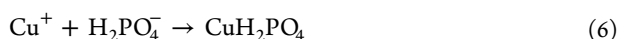
Figure 6. (a) Cycling performance of after-bending batteries with the LTO/Cu−N1 etched anode; (b) stability test of the LiB cell using LTO/Cu−N1 etched as the anode and LFP/Al as the cathode at 1 A g^{-1} (solid circle: charge capacity; hollow circle: discharge capacity); (c) flexible lithium-ion battery using LTO/Cu−N1 etched as the anode and LFP/Al as the cathode under the bending stress test, showing the discharge capacities at 0.1C. (Jian-Ming Chiu took these photographs.)

relevant result, the charge-transfer resistance of LTO/Cu−N1 etched is around 35.67 Ω and that of LTO/Cu is 43.01 Ω. LTO/Cu−N1 etched reduces the charge-transfer resistance, refreshing the thinner copper foil.

2.3. Mechanism Insights on Different Etchants (N1 and N2). The copper etching process of the ferric chloride etchant (Cu Etch-N2) is the most widely used in various industrial fields.[16] It has lower toxicity, is controllable, and has rapid etching advantages.[17,18] The Cu etching mechanism of FeCl$_3$ is as follows[19]

$$Cu_{(s)} + FeCl_{3(aq)} \rightarrow CuCl_{(s)} + FeCl_{2(aq)} \qquad (2)$$

$$CuCl_{(s)} + 3Cl^-_{(aq)} \rightarrow (CuCl_4)^{3-}_{(aq)} \qquad (3)$$

We reserved a small amount of copper with the etchant of Cu Etch-N2 to make a lightweight LTO/Cu-etched film electrode in the LiB. The capacity cannot be determined by galvanostatic charge−discharge measurement. Due to chemical reactions between the FeCl$_{3(aq)}$ and the copper surface, an oxide layer of brown anhydrous cupric chloride (CuCl$_2$) is formed on the surface of the copper foil. This modified copper surface with CuCl$_2$ affects the original electron transport pathway. Therefore, the copper film of the LTO/Cu needs to complete removal at 25 °C for 40 min and is obtained (Cu thickness is 15 μm) by the etchant of Cu Etch-N2 and then transferred to a fresh copper foil to study the electrochemical property. Furthermore, in an acidic environment containing chloride ions, the etchant of Cu Etch-N2 may have a micro-etching behavior for TiO$_2$.[20] According to the above-mentioned concern, the candidate chemicals need good copper etching capability and high selectivity to the LTO film. At the same time, we selected another H$_3$PO$_4$-based copper etchant (Cu Etch-N1) for testing. The etching rate of the etchant of Cu Etch-N1 is at 25 °C for 0.375 μm/min, in which the mechanism of redox is as follows[21]

$$Cu \rightarrow Cu^+ + e^- \qquad (4)$$

$$H_3PO_4 \rightleftharpoons H^+ + H_2PO_4^- \qquad (5)$$

$$Cu^+ + H_2PO_4^- \rightarrow CuH_2PO_4 \qquad (6)$$

$$CuH_2PO_4 + H^+ \rightarrow Cu^{2+} + H_3PO_4 + e^- \qquad (7)$$

$$Cu^+ \rightarrow Cu^{2+} + e^- \qquad (8)$$

$$Cu^+ \rightarrow Cu^+(bulk) \qquad (9)$$

$$Cu^{2+} \rightarrow Cu^{2+}(bulk) \qquad (10)$$

Early work on the etching rate of amorphous titanium oxide (TiO$_2$) in phosphoric acid was done by Okazaki *et al.*[22] The etching rate is of approximately 1 nm/min with the immersion test of the TiO$_2$ film in 85% by weight H$_3$PO$_4$ at 80 °C.[23] In the previous study, the etching rate of TiO$_2$ was dependent on the concentration and temperature of H$_3$PO$_4$. Because the concentration of H$_3$PO$_4$ in the etchant of Cu Etch-N1 is less than 20% by weight and the operating temperature is at 25 °C, we expect to obtain extremely high selectivity for TiO$_2$.

2.4. Demonstration and Concept Extension. The charge−discharge cycling performance of the LTO/Cu−N1 etched coin cell after the electrode-bending condition with a bending radius of 3 mm around 50 cycles was performed to investigate cells' cycling stability under bending stress as shown in Figure 6a. The capacity of the LiB using LTO/Cu−N1 etched by the bending stress test shows a similar trend as the sample without the bending stress test, in which the initial Coulombic efficiency of the LiB using LTO/Cu−N1 etched based on the lightweight copper foil is over 88% (discharge capacity = 145.6 mA h/g and charge capacity = 129.02 mA h/g). To validate the real LiB applications of LTO/Cu−N1 etched, we fabricated a Li-ion full coin cell using commercial LFP (LiFePO$_4$) materials as the positive electrode (cathode) and LTO/Cu−N1 etched as the negative electrode (anode) to estimate the electrochemical performance. We observed the cycling performance in the voltage range of 1.0−2.5 V at a current density of 1000 mA g^{-1} (Figure 6b). By the bending stress test, the LTO‖LFP cell capacity retention during charge/discharge cycles with five cycles is not different. This is due to the excellent flexibility of the lightweight LTO/Cu−N1 etched electrodes, which are not broken or damaged when undergoing deformation (Figure 6c).

3. CONCLUSIONS

We demonstrated the effective fabrication method of a lightweight and high-energy-density LiB using an etching process LTO anode on a conventional copper foil. This technique can be used to fabricate as lightweight electrode by a simple procedure. The new LTO anode with a flexible current collector and low weight, high electrical conductivity, and flexibility significantly improved the electrochemical performance and energy capacity. Finally, it is expected that the progressive development of the flexible current collector and subsequent Si@C anode will be potential for the next-level flexible LiB with high-energy capacity.

4. EXPERIMENTAL SECTION

4.1. LTO Freestanding Film/LTO−Cu Foil Preparation. First, we prepared the slurry by mixing lithium titanate powder (LTO) (80%) with polyvinylidene fluoride (PVDF, from Union Chemical Ind. Co., LTD) (10%) and Super P (10%) in N-methyl-2-pyrrolidone (NMP, from Alfa Aesar). Second, after rigorously stirring for 2 h, the slurry was cast on a sheet of a Cu foil (Ubiq Tech Co., Ltd.) to form a uniform film and was dried at 80 °C for 2 h under a vacuum environment. Third, we placed the LTO film on the surface of two different etchants, denoted by H_3PO_4-based solution (Cu Etch-N1) and $FeCl_3$-based solution (Cu Etch-N2) (Hai-Bo Advanced Chem-Materials Co., Ltd.), for 40 min to etch the Cu foil. Last, we washed the free-standing LTO film with DI water and dried the film at 60 °C for 30 min under vacuum. The preparation method of the LTO cast on the Cu foil was the same as the LTO free-standing film with the substrate of the Cu foil (Ubiq Tech Co., Ltd.) and without the etching process.

4.2. Characterizations. A field-emission scanning electron microscope (FE-SEM, JSM-6500) was used to analyze the surface morphology and microstructure of LTO/Cu and LTO/Cu-etched samples. The short-range order crystal structure of LTO/Cu and LTO/Cu-etched from Raman spectra was obtained using MRS5000 Micro Raman Spectrometer 532 nm with a 125 mW DPSS laser (Rayleytek Co., Ltd). The as-prepared samples' crystal structure was characterized using an X-ray diffractometer (XRD, Bruker D2 Advance, Cu Kα, λ = 1.5406 Å) operated at 40 kV and 40 mA. Different etchant solutions were analyzed by titanium (Ti) by coupled plasma optic emission spectrometry (ICP-OES, Spectro Arcos, SPECTRO model Analytical Devices, Perkin Elmer OPTIMA-7300DV).

4.3. Electrochemical Measurements. The LTO/Cu and LTO/Cu-etched battery were constructed with CR 2032 coin-type cells (Ubiq Tech Co., LTD.), assembled in an argon-filled glovebox where moisture and oxygen levels were measured less than 1 ppm. The LTO/Cu and LTO/Cu-etched served as working electrodes, and lithium foils were employed as counter and reference electrodes. A Celgard 2325 triple layer of the PP/PE/PP membrane was used as a separator; the electrolyte was 1 M $LiPF_6$ in ethylene carbonate and diethylene carbonate (1:1, in volume ratio). The galvanostatic charge−discharge measurement was carried out using a Ubiq BAT-750B battery test system in the potential range of 1300−2500 mV (vs Li/Li⁺). After fabricating the LTO/Cu and LTO/Cu-etched battery, the battery rested for 12 h before the charging−discharging process. Constant current charging and discharging were used for all tests.

LiB cells were fabricated using the LFP/Al cathode and LTO/Cu−N1 etched anode separated by a commercial Celgard 2325 separator. An aluminum pouch was used for the pouch-type full cells. The Al and Ni lead tabs were attached to the cathode and anode fabrics, respectively. The LiB cells were charged to 2.5 V under CC conditions first and then maintained at a constant voltage (CV) of 2.5 V until the current dropped below 20% of the CC value (CC-CV charging mode). The LiB cells were discharged to 1.0 V under only CC conditions. The cyclic voltammetry (CV) was performed at a scan rate of 0.1 mV s⁻¹ over a range of 1000−2500 mV (vs Li/Li⁺) on the Autolab electrochemical station. Electrochemical impedance spectroscopy measurements were carried out from 0.1 Hz to 100 kHz using an amplitude of the 10 mV AC signal.

■ ASSOCIATED CONTENT

ⓈSupportingInformation

The Supporting Information is available free of charge at https://pubs.acs.org/doi/10.1021/acsomega.1c06704.

> XRD patterns, XRD patterns and the SEM image, and cross-sectional SEM image of LTO/Cu-N1 etched at different positions (PDF)

■ AUTHOR INFORMATION

Corresponding Author

Chen-Hao Wang − *Department of Materials Science and Engineering, National Taiwan University of Science and Technology, Taipei City 106335, Taiwan; Center of Automation and Control, National Taiwan University of Science and Technology, Taipei City 106335, Taiwan;* ⓘ orcid.org/0000-0003-2350-3287; Email: chwang@mail.ntust.edu.tw

Authors

Chih-Hung Chen − *Department of Materials Science and Engineering, National Taiwan University of Science and Technology, Taipei City 106335, Taiwan*

Jian-Ming Chiu − *Department of Chemical Engineering, National Taiwan University of Science and Technology, Taipei City 106335, Taiwan*

Indrajit Shown − *Department of Chemistry, Hindustan Institute of Technology and Science, Chennai, Tamil Nadu 603103, India*

Complete contact information is available at:
https://pubs.acs.org/10.1021/acsomega.1c06704

Author Contributions

[⊥]C.-H.C. and J.-M.C. equally contributed to this work.

Notes

The authors declare no competing financial interest.

■ REFERENCES

(1) Xia, Q.; Jabeen, N.; Savilov, S. V.; Aldoshin, S. M.; Xia, H. Black mesoporous Li4Ti5O12−δ nanowall arrays with improved rate performance as advanced 3D anodes for microbatteries. *J. Mater. Chem. A* **2016**, *4*, 17543−17551.

(2) Ni, M.; Sun, D.; Zhu, X.; Xia, Q.; Zhao, Y.; Xue, L.; Wu, J.; Qiu, C.; Guo, Q.; Shi, Z.; Liu, X.; Wang, G.; Xia, H. Fluorine Triggered Surface and Lattice Regulation in Anatase TiO 2− x F x Nanocrystals for Ultrafast Pseudocapacitive Sodium Storage. *Small* **2020**, *16*, 2006366.

(3) Yang, T.; Li, H.; Tang, Y.; Chen, J.; Ye, H.; Wang, B.; Zhang, Y.; Du, C.; Yao, J.; Guo, B.; Shen, T.; Zhang, L.; Zhu, T.; Huang, J. In situ observation of cracking and self-healing of solid electrolyte interphases during lithium deposition. *Sci. Bull.* **2021**, *66*, 1754−1763.

(4) Hu, L.; Choi, J. W.; Yang, Y.; Jeong, S.; La Mantia, F.; Cui, L.-F.; Cui, Y. Highly conductive paper for energy-storage devices. *Proc. Natl. Acad. Sci. U.S.A.* **2009**, *106*, 21490.

(5) Cui, L.-F.; Hu, L.; Choi, J. W.; Cui, Y. Light-weight free-standing carbon nanotube-silicon films for anodes of lithium ion batteries. *ACS Nano* **2010**, *4*, 3671−3678.

(6) Kim, S. W.; Cho, K. Y. Current collectors for flexible lithium ion batteries: A review of materials. *J. Electrochem. Sci. Technol.* **2015**, *6*, 1−6.

(7) Wang, J.-Z.; Chou, S.-L.; Chen, J.; Chew, S.-Y.; Wang, G.-X.; Konstantinov, K.; Wu, J.; Dou, S.-X.; Liu, H. K. Paper-like free-standing polypyrrole and polypyrrole-LiFePO4 composite films for flexible and bendable rechargeable battery. *Electrochem. Commun.* **2008**, *10*, 1781−1784.

(8) Liu, X. H.; Zhang, L. Q.; Zhong, L.; Liu, Y.; Zheng, H.; Wang, J. W.; Cho, J.-H.; Dayeh, S. A.; Picraux, S. T.; Sullivan, J. P.; Mao, S. X.; Ye, Z. Z.; Huang, J. Y. Ultrafast electrochemical lithiation of individual Si nanowire anodes. *Nano Lett.* **2011**, *11*, 2251−2258.

(9) Li, N.; Chen, Z.; Ren, W.; Li, F.; Cheng, H.-M. Flexible graphene-based lithium ion batteries with ultrafast charge and discharge rates. *Proc. Natl. Acad. Sci. U.S.A.* **2012**, *109*, 17360.

(10) Liu, S.; Wang, Z.; Yu, C.; Wu, H. B.; Wang, G.; Dong, Q.; Qiu, J.; Eychmüller, A.; David Lou, X. W. A Flexible TiO2(B)-Based Battery Electrode with Superior Power Rate and Ultralong Cycle Life. *Adv. Mater.* **2013**, *25*, 3462−3467.

(11) Koo, M.; Park, K.-I.; Lee, S. H.; Suh, M.; Jeon, D. Y.; Choi, J. W.; Kang, K.; Lee, K. J. Bendable inorganic thin-film battery for fully flexible electronic systems. *Nano Lett.* **2012**, *12*, 4810−4816.

(12) Meng, C.; Liu, C.; Chen, L.; Hu, C.; Fan, S. Highly flexible and all-solid-state paperlike polymer supercapacitors. *Nano Lett.* **2010**, *10*, 4025−4031.

(13) Nyholm, L.; Nyström, G.; Mihranyan, A.; Strømme, M. Toward flexible polymer and paper-based energy storage devices. *Adv. Mater.* **2011**, *23*, 3751−3769.

(14) Podsiadlo, P.; Kaushik, A. K.; Arruda, E. M.; Waas, A. M.; Shim, B. S.; Xu, J.; Nandivada, H.; Pumplin, B. G.; Lahann, J.; Ramamoorthy, A.; Kotov, N. A. Ultrastrong and stiff layered polymer nanocomposites. *Science* **2007**, *318*, 80−83.

(15) Lim, E. T.; Ryu, J. S.; Choi, J. S.; Chung, C. W. Evolution of etch profile of copper thin films in high density plasmas of alcohol-based gases. *Vacuum* **2019**, *167*, 145−151.

(16) Li, Y.; Shao, H.; Lin, Z.; Lu, J.; Liu, L.; Duployer, B.; Persson, P. O. Å.; Eklund, P.; Hultman, L.; Li, M.; Chen, K.; Zha, X.-H.; Du, S.; Rozier, P.; Chai, Z.; Raymundo-Piñero, E.; Taberna, P.-L.; Simon, P.; Huang, Q. A general Lewis acidic etching route for preparing MXenes with enhanced electrochemical performance in non-aqueous electrolyte. *Nat. Mater.* **2020**, *19*, 894−899.

(17) Choi, J.-C.; Lee, J.-H. Etching behaviors of Cu and invar for metal core PCB applications. *J. Nanosci. Nanotechnol.* **2017**, *17*, 7358−7361.

(18) Bryce, C.; Berk, D. Kinetics of the dissolution of copper in iron(III) chloride solutions. *Ind. Eng. Chem. Res.* **1995**, *34*, 1412−1418.

(19) Yonemura, M.; Matsumura, Y.; Ohba, M.; Okawa, H.; Fenton, D. E. Template Synthesis of Phenol-based Heterodinucleating Macrocycles with Dissimilar N(amine)2O2and N(imine)2O2Metal-binding Sites. *Chem. Lett.* **1996**, *25*, 601−602.

(20) Burns, D. W. MEMS wet-etch processes and procedures. In *MEMS Materials and Processes Handbook*; Ghodssi, R., Lin, P., Eds.; Springer: Boston, MA, 2011; pp 457−665.

(21) Ding, L.; Wu, P.; Cheng, J.; Niu, Y.; Song, Z.; Kong, X. Electrochemical oscillations during electro-oxidation of copper anode in phosphoric acid solution. *Electrochemistry* **2019**, *87*, 14−19.

(22) Okazaki, S.; Ohhashi, T.; Nakao, S.; Hirose, Y.; Hitosugi, T.; Hasegawa, T. Wet Etching of Amorphous TiO2Thin Films Using H3PO4-H2O2Aqueous Solution. *Jpn. J. Appl. Phys.* **2013**, *52*, 098002.

(23) Cumba, L. R.; Bicalho, U. D. O.; Do Carmo, D. R. Preparation and voltammetric studies of titanium (IV) phosphate modified with silver hexacyanoferrate to an electroanalytical determination of L-cysteine. *Int. J. Electrochem. Sci.* **2012**, *7*, 4465−4478.